NOTICE CONCERNING COPYRIGHT RESTRICTIONS

Difference Between Steam-Water and Air-Water Relative Permeabilities in Fractures

Chih-Ying Chen*, Kewen Li and Roland N. Horne

Stanford Geothermal Program, Department of Petroleum Engineering
Stanford University, Stanford, CA, 94305-2220 USA
***e-mail: alnchen@stanford.edu**

Keywords

Steam-water relative permeability; Fracture flow

ABSTRACT

The goal of this research has been to compare steam- and air-water transport through fractured media and gain better understanding of the behaviors of relative permeability in fractures. Air-water (or nitrogen-water) relative permeabilities are often used for geothermal reservoir simulations while steam-water relative permeabilities in fractures are rarely measured owing to difficulties and complexities of steam-water experiments. A novel and accurate methodology was developed to capture the unstable nature of the steam-water flow in a smooth-walled fracture. Repeatable results were obtained and show that steam-water relative permeabilities are different from nitrogen-water relative permeabilities. The average steam-water relative permeabilities show less phase interference. Also, comparing with previous research into air-water relative permeabilities in fractures, both average steam- and nitrogen-water relative permeabilities were seen to behave closer to the X-curve.

Introduction

In geothermal reservoirs, the fluids, steam and water, are both derived from the same substance but in different phases. The phase change during steam-water flow is a physical phenomenon that does not occur in the multiphase flow of distinct fluids such as air and water, hence the multiphase flow properties are likely to differ. Also, the phase change during steam-water multiphase flow has made it difficult to investigate steam-water relative permeability. Even in multiphase flow without boiling, few published data are available for two-phase flow in fractures. Most of the studies have been done for air-water systems or for water-oil systems.

One of the most commonly used approaches to model multiphase flow in fractures is the porous medium approach. This approach treats fractures as connected two-dimensional porous media. In this model, a pore space occupied by one phase is not available for flow for the other phase. A phase can move from one position to another only upon establishing a continuous flow path for itself. As in porous media, the competition for pore occupancy is described by relative permeability and governed by Darcy's law. Darcy's law for single-phase liquid system is:

$$u_l = \frac{k_{abs}(p_i - p_o)}{\mu_l L} \tag{1}$$

where subscript l stands for the liquid phase, i for inlet and o for outlet; μ, p, L, u, k_{abs} are the viscosity, pressure, fracture length, Darcy flow velocity and absolute permeability respectively.

For liquid phase in two-phase flow, Eq. 1 becomes

$$u_l = \frac{k_{abs}k_{rl}(p_i - p_o)}{\mu_l L} \tag{2}$$

where krl is the relative permeability of the liquid phase.

Similarly, Darcy's law derived for single-phase isothermal gas flow in porous media (Scheidegger, 1974) is:

$$u_g = \frac{k_{abs}k_{rg}(p_i^2 - p_o^2)}{2\mu_g L p_o} \tag{3}$$

with the subscript g pertaining to the gas phase. In two-phase flow, Eq. 3 becomes

$$u_g = \frac{k_{abs}k_{rg}(p_i^2 - p}{2\mu_g L p_o} \tag{4}$$

with krg as the gas relative permeability.

The absolute permeability of a smooth-walled fracture is a function only of the fracture aperture, b (Witherspoon et al., 1980) as described in the relationship:

$$k_{abs} = \frac{b^2}{12} \tag{5}$$

For gas-water two-phase flow, the sum of the relative permeabilities, k_{rl} and k_{rg} indicates the extent of phase interference. A sum of relative permeabilities equal to one means the absence of phase interference. Physically this implies that each phase flows in its own path without impeding the flow of the other. The lower is the sum of the relative permeabilities below 1, the greater is the

phase interference. Relative permeability functions are usually taken to be dependent on phase saturation. The two most commonly used expressions for relative permeability for homogeneous porous media are the X-curve and the Corey curve (Corey, 1954). The X-curve defines relative permeability as a linear function of saturation:

$$k_{rl} = S_l \tag{6}$$

$$k_{rg} = S_g \tag{7}$$

where S_l and S_g are the liquid and gas saturation respectively. The Corey curves relate relative permeability to the irreducible or residual liquid and gas saturation, S_{rl} and S_{rg} :

$$k_{rl} = S^{*4} \tag{8}$$

$$k_{rg} = (1-S^*)^2(1-S^{*2}) \tag{9}$$

$$S^* = (S_l - S_{rl})/(1-S_{rl}-S_{rg}) \tag{10}$$

Previous work on multiphase flow in fractures includes Romm's (1966) experiment with kerosene and water through an artificial parallel-plate fracture lined with strips of polyethylene or waxed paper. Romm found a linear relationship between permeability and saturation, $S_w = k_{rw}$, $S_{nw} = k_{rnw}$ such that $k_{rw}+k_{rnw} = 1$ which represents the X-curve behavior. Persoff et al. (1991) did experiments on gas and water flow through rough-walled fractures using transparent casts of natural fractured rocks. The experiment showed strong phase interference similar to the flow in porous media. In the experiments of both Persoff (1991) and Persoff and Pruess (1995), flow of a phase was characterized by having a localized continuous flow path that is undergoing blocking and unblocking by the other phase. Diomampo (2001) performed experiments of nitrogen and water flow through both smooth- and rough-walled artificial fractures. The relative permeability data of these published results are compared in Figure 1 against commonly used relative permeability relations for porous media, the X-curve and Corey curve.

These previous studies show a diversity of behavior of nonboiling relative permeabilities in fractures. However, the X-curve is commonly used in geothermal reservoir simulation,

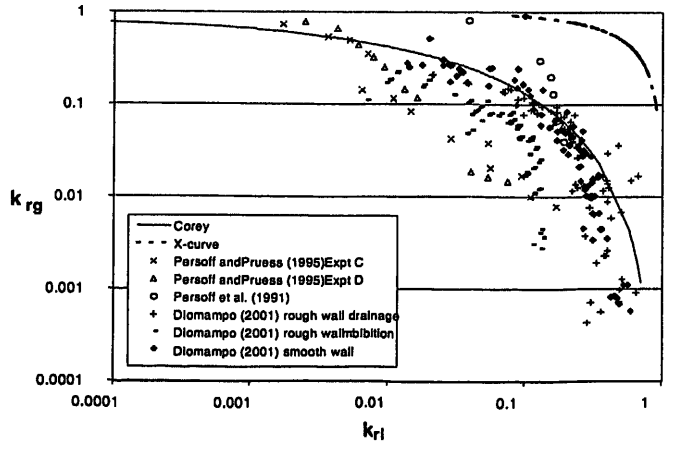

Figure 1. Compendium of previous measurements of air-water relative permeabilities in fractures (from Diomampo, 2001).

which shows a contradiction with most previous measurements other than Romm's (1966). Presently, the flow mechanism and the characteristic behavior of relative permeability in fractures are still not well determined. Issues such as whether a discontinuous phase can travel as discrete units carried along by another phase or will be trapped as residual saturation as in porous medium are unresolved. The question of phase interference, i.e. whether the relative permeability curve against saturation is described by an X-curve, Corey or some other function, is still unanswered. The main objective of this study was to contribute to the resolution of these issues.

Experimental Methodology

The whole experiment system is illustrated in Figure 2, which shows the deaerated water supply, the fracture apparatus (inside the air bath), back-pressure device, data acquisition system, and digital image recording.

Fracture Apparatus Description

The fracture is created by a smooth glass plate on top of an aluminum plate, confined by a metal frame bolted to the bottom plate. Details of the fracture design were described in Diomampo (2001) and Chen et al. (2002). The complete improved measurement configuration in the fracture apparatus and its picture are

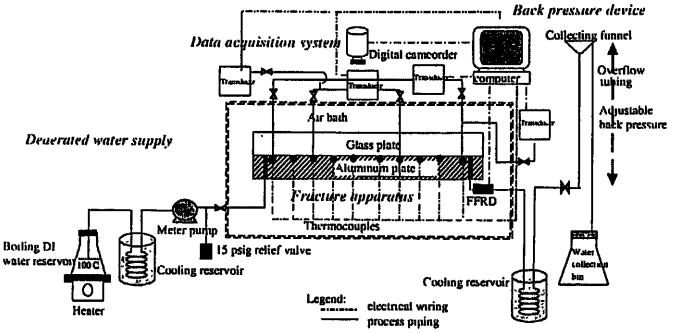

Figure 2. Process flow diagram for steam-water experiment.

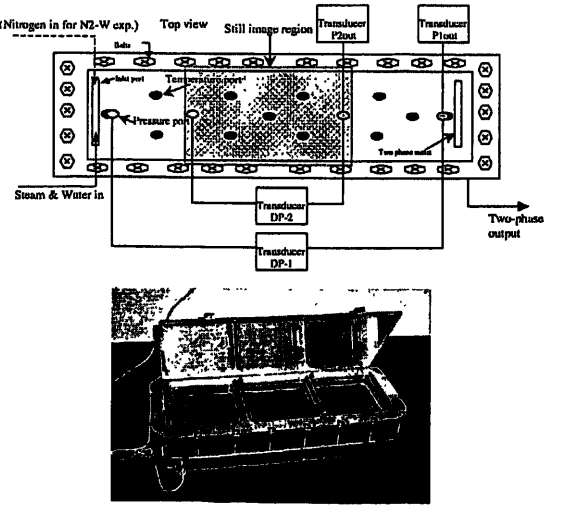

Figure 3. Schematic diagram and picture of fracture apparatus.

shown in Figure 3. In the experiments, pressure ports were drilled along the fracture for intermediate pressure difference measurement to minimize capillary end effect and to facilitate intermediate absolute pressure measurement through the fracture.

Fractional Flow Ratio Detector (FFRD

One of the main challenges of the steam-water flow experiment was to measure the steam and water flow rates, since there is phase transition occurring when steam and water flow through the fracture. Therefore using flow meters to measure the rate of each phase becomes inappropriate, because it is always impossible to separate steam from water without any mass loss or gain. To overcome this situation, a fractional flow ratio detector (FFRD) was designed and constructed as shown in Figure 4. The principle of the FFRD is that different phases will have different refractive indices. A phototransistor (NTE 3038, NPN-Si, Visible) was installed inside the FFRD, producing different voltages when sensing different strengths of light. The water phase produces a higher voltage when flowing through the FFRD. Once the steam and water responses are obtained from the FFRD, the steam and water phase flow ratios are obtained by determining the ratio of the number of steam and water signals. Once the outlet steam and water fractional flow ratio, f_s and f_w, are obtained, it is easy to evaluate $q_{out,s}$ and $q_{out,w}$ by using mass balance if a steady-state condition is reached. The calibration of the FFRD is shown in Figure 5. The detail of this device can be found in Chen et al. (2003).

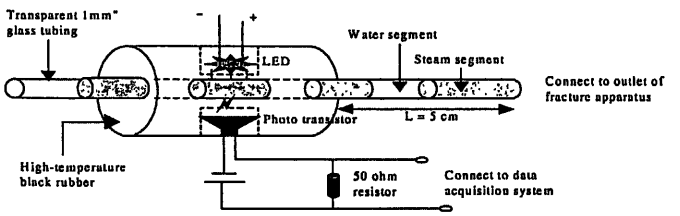

Figure 4. Schematic of fractional flow ratio detector (FFRD).

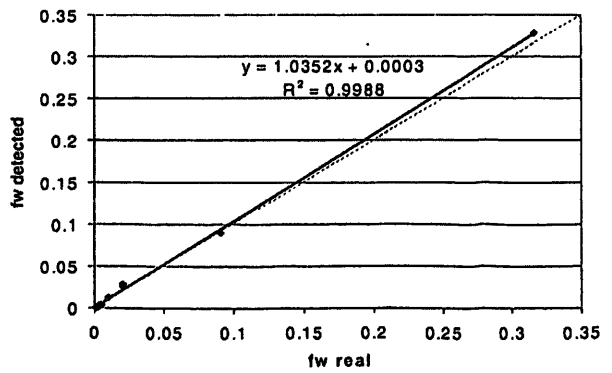

Figure 5. FFRD calibration with FFRD tubing ID: 1.0mm.

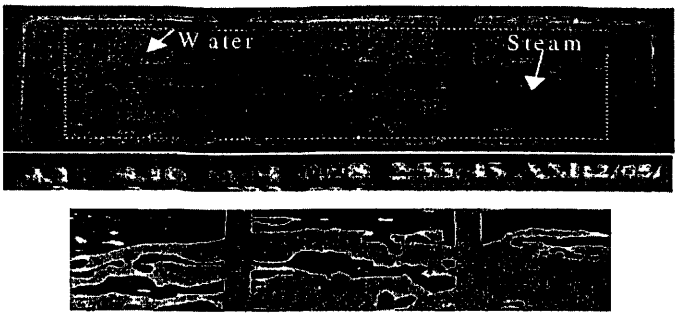

Figure 6. Comparison between the true color image of the fracture flow and gray scale image from Matlab QDA program used in measuring saturation.

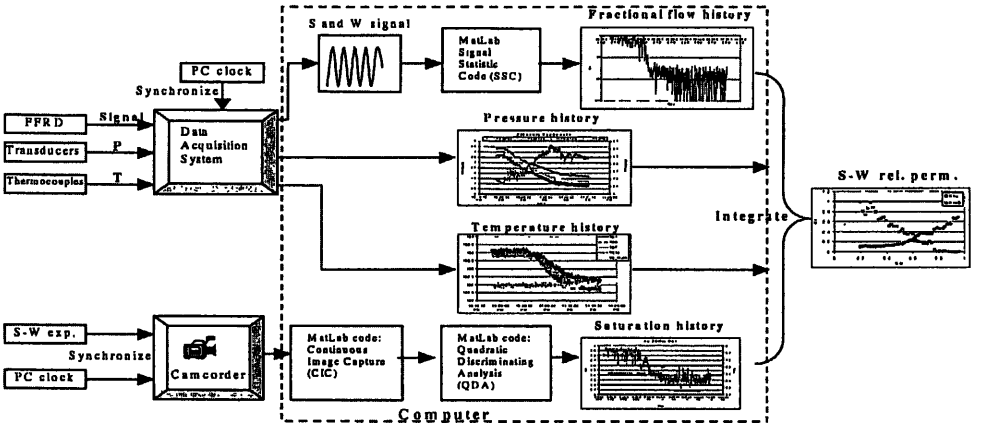

Figure 7. Data and signal processing flowchart.

Saturation

Still images were extracted from digital video recorded during the experiments. The photographs were processed in a Matlab® program. The program does quadratic discriminant analysis (QDA) to group the pixels of the picture into three groups: the water phase, steam phase and the frame. The grouping is based on color differences. Saturation is calculated as total pixels of the liquid group over the sum of the steam and liquid groups. Figure 6 is a comparison of the gray-scaled image produced by the QDA program and the original photograph from the digital camcorder. The detail of this technique was described in Diomampo (2001) and in Chen et al. (2003). The methodology used to integrate all the data and signals and then calculate the steam-water relative permeabilities is illustrated in the flow chart in Figure 7.

Experimental Results and Discussion

Four experiments were conducted for different purposes. These experiments were: (1) the steady-state nitrogen-water experiment at room temperature (24°C); (2) steady-state nitrogen-water experiment at high temperature (90°C); (3) unsteady steam-water experiment (also in Chen, 2002), and (4) steady-state steam-water experiment. The aperture of the fracture was 0.13mm except in the unsteady steam-water experiment (in which the aperture was 0.076mm). Before the experiment, the absolute permeability of the smooth-walled fracture was measured. As can be seen in Figure 8, with the 0.13mm fracture aperture, the absolute permeability

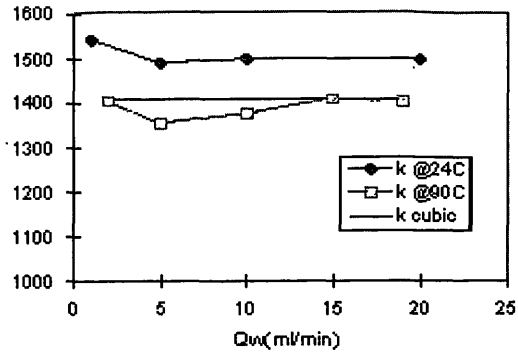

Figure 8. Absolute permeability of the smooth-walled fracture (aperture = 0.13mm) at different temperature and water rates.

of the fracture measured is around 1505 darcies at 24°C and 1387 darcies at 90°C when the water rates are less than 20ml/min. While applying the cubic law from Eq. 5, the permeability estimated is around 1400 darcies. This is close to our measurement.

Nitrogen-Water Experiments

More than 3000 still images were extracted from the digital video and used for the flow pattern characterization and saturation calculation in each experiment. Several types of flow patterns observed under high, intermediate, and low water saturation are shown in Figure 9, 10 and 11 respectively. Each figure shows four consecutive images. Figure 9 shows the nitrogen-water flow under high water saturation at 24°C (left) and 90°C (right). Nitrogen moves in narrow slugs and flows discontinuously because of the relatively low gas flow rate. The higher pressure drop happens mostly when a slug tries to break through the water region. Once the slug reaches the outlet of the fracture, the pressure drop decreases. This type of slug movement was seen frequently in high water saturation situations.

Figure 10 shows the nitrogen-water flow at intermediate water saturation. Unlike the high water saturation case, the gas forms its own stable flow path through the fracture and gas and water behave nearly like layer flows under intermediate water saturation. At room temperature, most of the gas flows in the upper region of the fracture, while most of the water flows in the lower. At high temperature, almost all of the gas flows solely in the center region

Figure 9. The continuous nitrogen-water flow behavior in smooth-walled fracture at 24°C (left) and 90°C (right) under high water saturation (~90%) (nitrogen phase is dark, water phase is light).

Figure 10. The continuous nitrogen-water flow behavior in smooth-walled fracture at 24°C and 90°C under intermediate water saturation (~40%).

Figure 11. The continuous nitrogen-water flow behavior in smooth-walled fracture at 24°C and 90°C under low water saturation (~15% left, ~5% right).

of the fracture, while most of the water flows above and below the gas path. Except for a small amount of immobile water inside the central gas channel, the gas path is more uniform and is not tortuous in comparison with the room temperature case. If a longer time scale is used to observe the behavior, some gas channels are seen to be blocked, and some are seen to be unblocked by water. In other words, the gas flow path undergoes continuous snapping and reforming due to the invasion of water.

Figure 11 shows the nitrogen-water flow under low water saturation. At room temperature, water flows through some narrow paths and sometimes as slow slugs as shown in the left figure. The pressure drop along the fracture is fairly stable in this condition. Comparing the high temperature case to the room temperature case, it is clear that the water saturation is much smaller than that in the room temperature case when input rates are the same (Qw=0.5*ml/min* and Qg=200*ml/min* in both cases). The instantaneous f_w sensed was also smaller than that in room temperature case. Consequently, some water evaporated into gas phase during the two-phase flow due to the high temperature and relatively large gas flow rate. It is necessary to evaluate the evaporation rate and the steam ratio in the gas phase since the gas phase contains not only nitrogen but also some amount of water vapor in this high-temperature case.

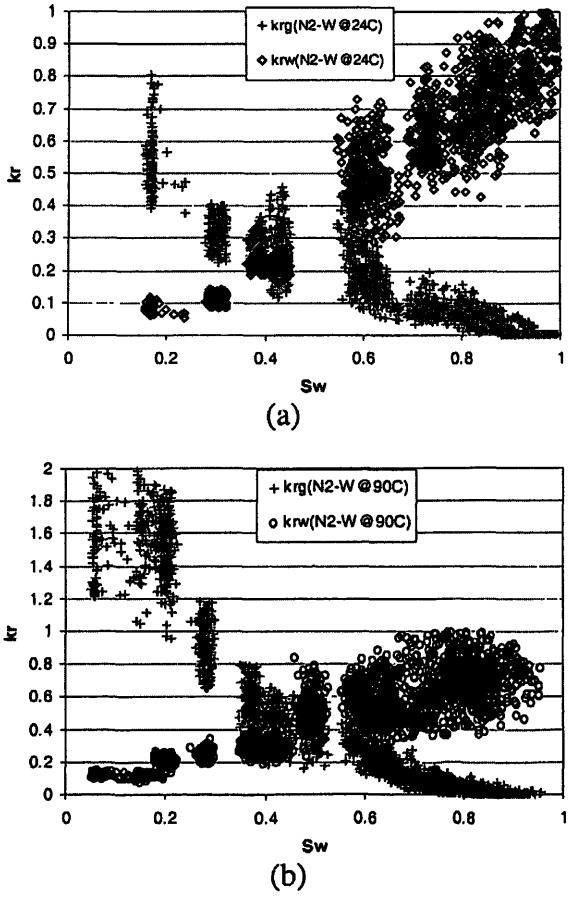

Figure 12. Comparison of comprehensive nitrogen-water relative permeabilities between 24°C (a) and 90°C (b) in the smooth-walled fracture.

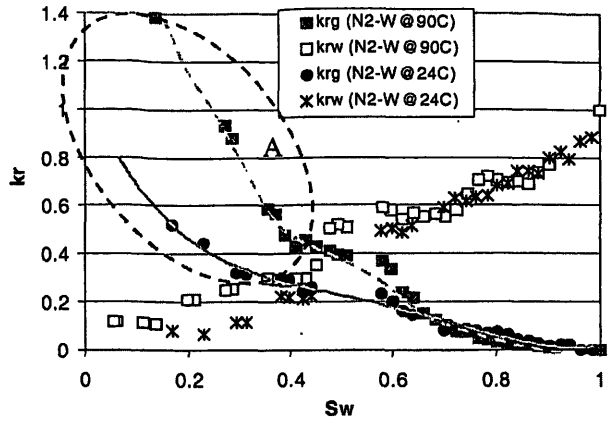

Figure 13. Comparison of average nitrogen-water relative permeabilities between 90°C and 24°C.

Comprehensive nitrogen-water relative permeabilities at room (24°C) and high temperature (90°C) are shown in Figure 12(a) and (b) respectively. Data points from room temperature and high temperature cases show acceptable correlation. In both cases, comprehensive water relative permeabilities are scattered under high water saturation owing to the slug flow in the gas phase as shown in Figure 9. The vertical scattered effect in the gas relative permeabilities under extremely low water saturation may be associated with either the pressure fluctuation due to the slow moving water slugs as shown in Figure 11 or the difficulty in sensing the instantaneous f_w from the FFRD at low f_w. Overall, nitrogen-water relative permeability values at 90°C are greater than those at 24°C.

Figure 13 shows moving window averages of the full results shown in Figure 12. The trend lines in Figure 13 are to facilitate the comparison only. The water-phase relative permeability values at these two different temperatures are close and behave almost the same as the water part of the X-curve (linear line with slope=1). The gas-phase relative permeability values at these two different temperatures show different behaviors. It is evident that the gas curve at 90°C is higher than that at 24°C. It is worth noting that in the 90°C case, there is a strong effect of evaporation from the water phase which increases the magnitude of the gas. Therefore, there is not only pure nitrogen but also water vapor in the gas phase. The gas viscosity used in Eq. 4 has to be the mixture-gas viscosity instead of the pure nitrogen viscosity. The viscosity of the mixture of nitrogen and water vapor can be expressed as:

$$\mu_{mix,g} = \frac{\mu_{N2,g} Q_{N2,g} + \mu_{w,g} Q_{w,g}}{Q_{N2,g} + Q_{w,g}} \tag{11}$$

where, $\mu_{N2,g}$ and $\mu_{w,g}$ are the nitrogen viscosity and water vapor viscosity respectively; $Q_{N2,g}$ and $Q_{w,g}$ are the nitrogen volumetric rates and water vapor volumetric rates which will be calculated from the water evaporation rate, X obtained from Eq. 12. In Figure 13, when water saturation is less than 0.5, the gas-phase relative permeability values at 90°C show a more significant increasing trend in comparison to the case of 24°C. This difference may be attributed to the increase of the steam ratio because of the strong evaporation effect at 90°C. However, it might be questionable that the gas-phase relative permeability values near the end point are more than unity in the 90°C case. This overestimated behavior can be attributed to both the unstable thermodynamic properties

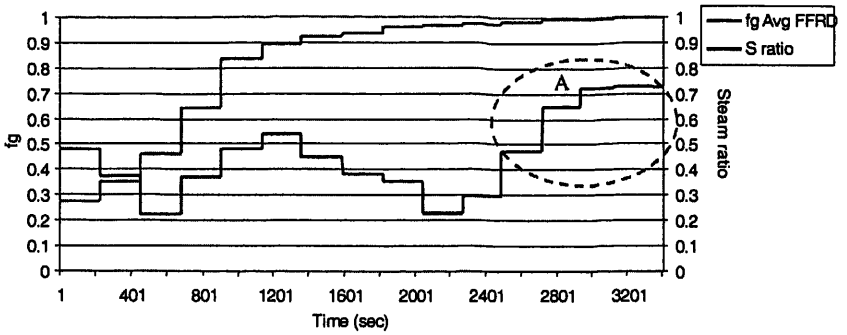

Figure 14. Steam ratios versus gas fraction flow in the nitrogen-water experiment at 90°C.

due to the evaporation effect and the overestimation of gas flow rates measured from the outlet of the fracture.

The instantaneous fractional flow of water, f_w, obtained from the FFRD can be used to calculate evaporation rate, X, given input water and gas (nitrogen) rates. By using the mass balance theory, X can be calculated by Eq. 12:

$$X = \frac{Q_{w0,l} - f_w(Q_{w0,l} + Q_{N2,g})}{1 + f_w(\frac{v_{w,g}}{v_{w,l}}) - f_w} \tag{12}$$

where, $Q_{w0,l}$ and $Q_{N2,g}$ are the input liquid water rate and gas rate respectively; $v_{w,l}$ and $v_{w,g}$ are the specific volume for water and steam (or water vapor) at some specific temperature; f_w is the instantaneous water fractional flow measured by the FFRD. Figure 14 shows the gas fractional flow, f_g, versus the steam ratio which is the volume of the steam evaporated from the water phase to the total volume of gas (sum of the input gas and produced steam). It is clear that water can evaporate to the vapor phase in the nitrogen-water experiment at 90°C, especially in a high gas rate situation. As shown in part A in Figure 14, when gas fractional flow, f_g, is close to 1, the steam ratio reaches 0.73. This corresponds to part A in Figure 13. This indicates that the more water vapor in the gas phase, the higher the gas-phase relative permeability values. Essentially, average relative permeability curves at both 24°C and 90°C show less phase interference compared to the general relative permeability curves in porous media (Corey-type curves).

Figure 15. The continuous steam-water flow behavior in smooth-walled fracture under high water saturation (~90%). (steam phase is dark, water phase is light).

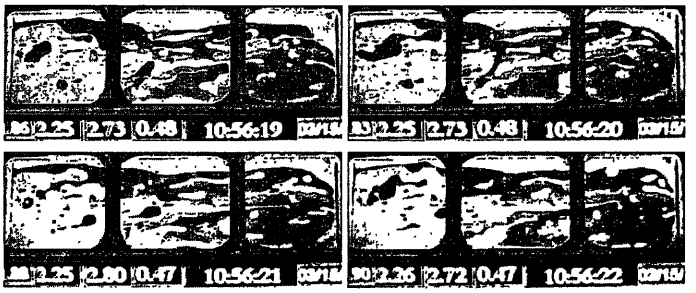

Figure 16. The continuous steam-water flow behavior in smooth-walled fracture under intermediate water saturation (~40%).

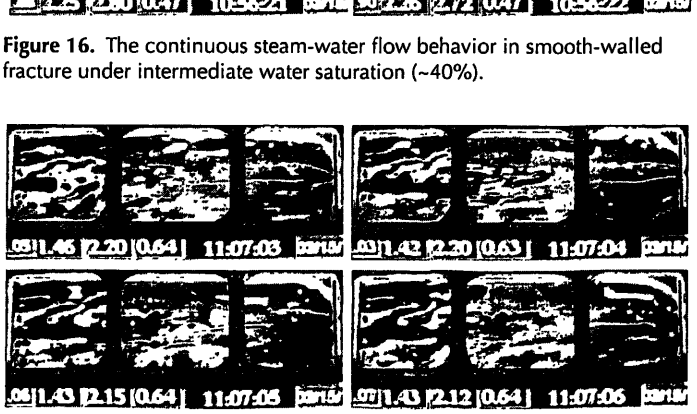

Figure 17. The continuous steam-water flow behavior in smooth-walled fracture under low water saturation (~20%).

Steam-Water Experiments

The unsteady and steady-state steam-water relative permeability experiments were conducted at around 104°C. The procedure and detail of the unsteady steam-water relative permeability experiment were described in Chen et al. (2002). The procedure of the steady-state experiment is similar to the unsteady experiment, except data were obtained when the steam-water flow reached steady state, or underwent repeatable flow regime changes even though the flow was unstable. The flow regime under high water saturation conditions behaved similar to the nitrogen-water case. As can be seen in Figure 15, the steam phase flows in fast moving slugs. The shape of slugs is more amorphous than that in the nitrogen-water case. The steam-water flow behavior is different from that of the nitrogen-water case under intermediate and low water saturations. As illustrated in Figures 16 and 17, the steam can flow via slugs, bubbles, and channels. On the other hand, the water flows via water slugs, water bubbles, and water channels. Even under the low water saturation conditions, the steam-water flow is still unstable. The steam phase and water phase can flow together in several different forms. This two-phase cocurrent flow situation was rarely seen in the nitrogen-water case.

Figure 18(a) and (b) show comprehensive steam-water relative permeabilities from both unsteady and steady experiments. The k_{rw} values behave smoothly in both cases, whereas the k_{rs} values are more scattered in the unsteady case. This might be because the error and uncertainty increase when steam-water flow is in unsteady condition. The major errors in the unsteady experiments are the delay of f_s and f_w measurement from the FFRD, the FFRD detection limit, and the pressure fluctuation in the unstable high-temperature fracture flow. The steady-state experiment was conducted after improving the FFRD detection limit and pressure fluctuation problems; therefore, a more correlated result was expected in the steady experiment. Comparing Figure 18 to Figure 12, comprehensive steam-water relative permeabilities show more

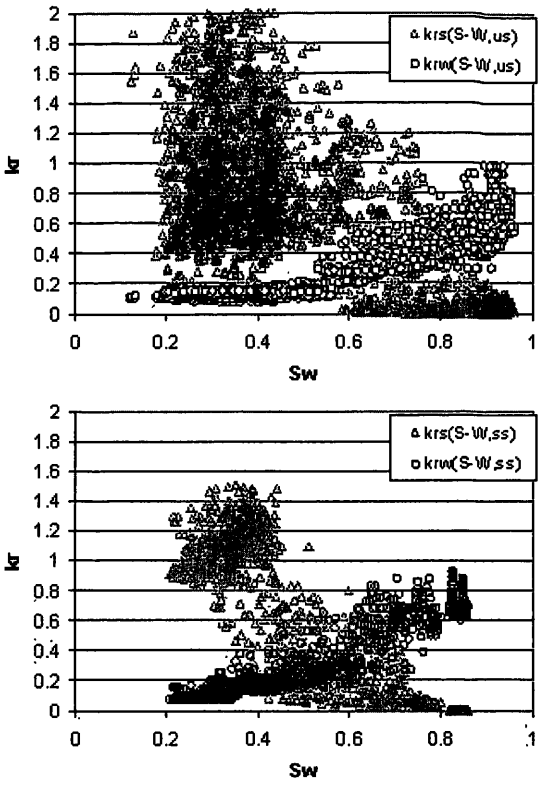

Figure 18. Comprehensive steam-water relative permeabilities in both unsteady (a) and steady-state (b) experiments.

scattered than nitrogen-water case in general. Nevertheless all of these four results (nitrogen-water at 24°C, nitrogen-water at 90°C, unsteady steam-water, steady steam-water experiments) are all scattered in different magnitude. This scattered effect could be associated with the fluctuating and unstable nature of the multi-phase flow in fractures.

Averages of the relative permeabilities over 2% saturation ranges from Figure 18(a) and (b) are shown in Figure 19, while the lines in Figure 19 are to facilitate the comparison only. The figure shows good correlation in both steam and water curves. Basically, the unsteady results are similar to the steady case, and the end points of these two experiments are close. However, the gas curve in the unsteady experiment shows less convexity than that in

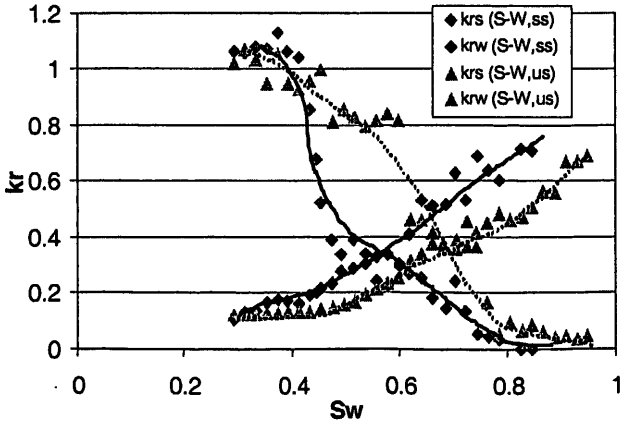

Figure 19. Steam-water relative permeabilities in both unsteady and steady-state experiments by applying 2% Sw averages.

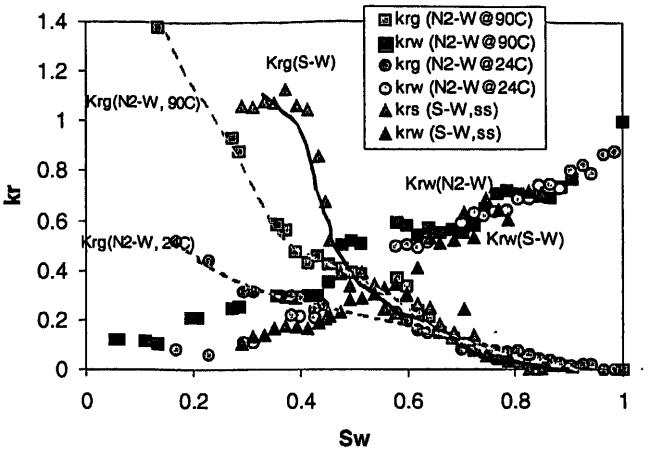

Figure 20. Comparison of relative permeability curves between steam- and nitrogen-water cases in the smooth-walled fracture.

the steady case, while the water curve in the unsteady experiment is slightly lower than in the steady case. These differences in the unsteady results can be attributed to the measurement errors due to the unsteady experimental conditions and the technical problems in the FFRD as mentioned before. Steam-water relative permeability curves show less phase interference and are not close to the Corey-type relative permeability behavior.

Figure 20 compares window averages of relative permeabilities between steady steam- and nitrogen-water cases in the smooth-walled fracture. Liquid curves have almost identical trends except at low water saturation ranges where the steam-water case may lose some accuracy because of the detection limit of the FFRD. On the other hand, the gas curves behave very differently. The steam curve shows a much more mobile character than the nitrogen curve, which can be seen from the higher relative permeability values in the steam curve in Figure 20. This phenomenon was also observed from the digital images. The nitrogen curve at 90°C is higher than that at 24°C. This shows the consistency with some theoretical research and some experimental measurements in porous media. In spite of this, the nitrogen-water experiment at 90°C and the steam-water experiment might overestimate the gas-phase relative permeabilities because of the overestimation of the gas rates as described before. The gas flow rates correction by using image processing approaches is in progress.

Figure 21, overleaf, summarizes the recent measurements of gas-water relative permeabilities in fractures in comparison to a collection of previously published results. Comparing the current results with previous measurements of air-water relative permeabilities in fractures, both steam- and nitrogen-water values from this research behave close to X-curve, which represents a behavior different from previous published measurements. Most of the previously published results proposed that air-water relative permeabilities in fractures follow the Corey-type curve or lie below it. It is necessary to mention that some of fractures in these studies were rough-walled. Currently, the roughness of the fracture was not been considered in this research. On the other hand, Romm (1966) also found similar X-curve behavior in his experiment with kerosene and water through an artificial smooth parallel-plate fracture lined with strips of polyethylene or waxed paper.

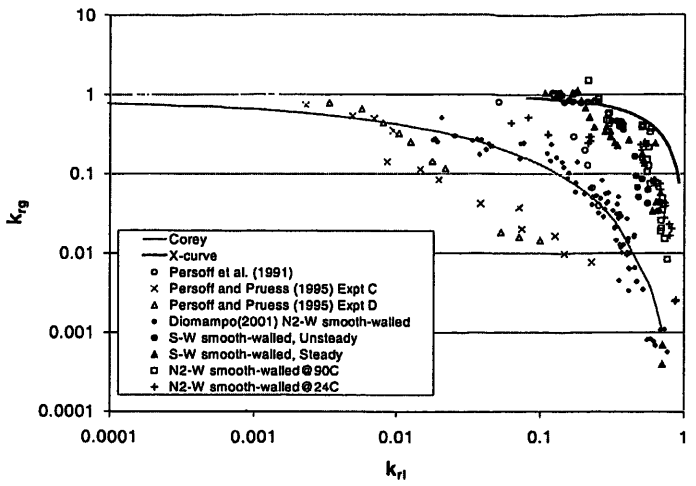

Figure 21. Comparison of steam- and nitrogen-water relative permeabilities in this research with previous measurements of air-water relative permeabilities in fractures.

Conclusion

1. The steam-water flow behavior in fractures is different from that of nitrogen-water flow. This is particularly obvious in low water saturation conditions. The steam and water can flow concurrently in the smooth-walled fracture; contrarily, nitrogen and water have the tendency to block each other.
2. Steam-water relative permeabilities are different from nitrogen-water relative permeabilities in the smooth-walled fracture. Steam-phase curves show less phase interference in comparison to the nitrogen-phase curves while the water-phase curves are relatively similar.
3. Comparing with previous research into air-water relative permeabilities in fractures, both average steam- and nitrogen-water relative permeabilities behave closer to the X-curve in this research, which is consistent with the result from Romm (1966) but is in contradiction to some recently published measurements.
4. The temperature effect on nitrogen-water relative permeabilities is evident in the gas-phase curves. The higher gas-phase curve at 90°C is partially due to the effect of the evaporated steam. This also reconfirms that the steam phase is more mobile than the nitrogen phase.
5. Comprehensive relative permeability plots show more scatter in the steam-water experiments. Furthermore, the steam-water flow seldom forms stable paths as observed from the digital images and videos. This indicates the unsteady nature of steam-water flow in fractures.

Acknowledgement

This research was supported by the US Department of Energy under contract DE-FG07-02ID14418. The fracture apparatus was originally designed by the former MS student Gracel Diomampo and technician Will Whitted who are gratefully acknowledged.

References

Chen, C.-Y., Diomampo, G., Li, K. and Horne, R.N., 2002. "Steam-Water Relative Permeability in Fractures," *Geothermal Resources Council Transactions Vol.26*, p. 87-94.

Chen, C.-Y., Li, K. and Horne, R.N., 2003. "Steam-Water Relative Permeability in Fractures," Quarterly Report for Jan-Mar. 2003, Stanford Geothermal Program, Stanford University, p. 1-30.

Corey, A.T., 1954. "The Interrelations Between Gas and Oil Relative Permeabilities," *Producers Monthly* Vol. 19, p. 38-41.

Diomampo, G.P., 2001. "Relative Permeability through Fractures," MS thesis, Stanford University, Stanford, California.

Horne, R.N., Satik, C., Mahiya, G., Li, K., Ambusso, W., Tovar, R., Wang, C., and Nassori, H., May 28-June 10, 2000. "Steam-Water Relative Permeability," *Proc. of the World Geothermal Congress* 2000, Kyushu-Tohoku, Japan.

Kncafsy, T. J. and Pruess, K., December 1998. "Laboratory Experiments on Heat-Driven Two-Phase Flows in Natural and Artificial Rock Fractures," *Water Resources Research* Vol. 34, No. 12, p. 3349-3367.

Lockhart, R. W. and Martinelli, R.C., 1949. "Proposed Correction of Data for Isothermal Two-Phase Component Flow in Pipes," *Chem. Eng. Prog.*, Vol. 45, No. 39.

Persoff, P. K., Pruess, K. and Myer, L., January 23-25 1991. "Two-Phase Flow Visualization and Relative Permeability Measurement in Transparent Replicas of Rough-Walled Rock Fractures," *Proc. 16th Workshop on Geothermal Reservoir Engineering*, Stanford University, Stanford, California.

Persoff, P., and Pruess, K., May, 1995 "Two-Phase Flow Visualization and Relative Permeability Measurement in Natural Rough-Walled Rock Fractures," *Water Resources Research* Vol. 31, No. 5, p. 1175-1186.

Pruess, K., and Tsang, Y. W., September 1990. "On Two-Phase Relative Permeability and Capillary Pressure of Rough-Walled Rock Fractures," *Water Resources Research* Vol. 26 No. 9, p. 1915-1926.

Romm, E.S., 1966. "Fluid Flow in Fractured Rocks", "Nedra" Publishing House, Moscow (Translated from the Russian).

Scheidegger, A.E., 1974. *The Physics of Flow Through Porous Media*, 3rd ed., University of Toronto, Toronto.

Witherspoon, P.A., Wang, J.S.W., Iwai, K. and Gale, J.E., 1980. " Validity of Cubic Law for Fluid Flow in a Deformable Rock Fracture," *Water Resources Research*, Vol. 16, No. 6, p. 1016-1024.